DOI: https://doi.org/10.24297/jap.v23i.9785

Study on momentum density in semiconductor compounds AlBi, InBi, and GaBi by positron annihilation

O. Benkraouda, M. Benkrauda and N. Amrane,*

United Arab Emirates University Faculty of Science

Physics Department

Al Ain P.O. Box 1555,1 United Arab Emirates

E-mail: namrane@uaeu.ac.ae

Abstract

The independent particle model (IPM) coupled with empirical pseudopotential method (EPM) was used to compute the thermalized positron charge densities in specific family of binary tetrahedrally coordinated crystals of formula A^NB^{8-N}. Initial results show a clear asymmetrical positron charge distribution relative to the bond center. It is observed that the positron density is maximum in the open interstices and is excluded not only from the ion cores but also to a considerable degree from the valence bonds. Electron-positron momentum densities are calculated for the (001,110) planes. The results are used to analyze the positron effects in InBi, AlBi, and GaBi. Our computational technique provides the theoretical means of interpreting the k-space densities obtained experimentally using the two-dimensional angular correlation of annihilation radiation (2D-ACAR).

Keywords: band structure, charge density, positron annihilation, momentum density.

*Corresponding author: namrane@uaeu.ac.ae

1 Introduction

Topological insulators (TIs) have captured unprecedented scientific and technological interests in the past few years [1-5]. Two-dimensional (2D) TIs, known as quantum spin Hall (QSH) insulators, provide small bandgap edge states with the protection of time-reversal symmetry, which ensures the propagation direction of electrons on the surface locked to their spin orientation [6-8]. However, due to the small bandgaps, group IV 2D materials such as graphene [9], Silicene and Germanene [10-12], operate impracticably at room temperature. Recently, potential QSH insulator materials with large bandgaps were found to be promising building blocks for novel coherent spin transport related devices [13-15].

The binary compounds of group III elements and bismuth with buckled honeycomb structure have been studied and predicted to have large bandgaps due to the large spin–orbit coupling (SOC) effect of Bi atoms, which is desirable for room-temperature spintronic applications. Among these 2D sheets, only GaBi, InBi and TlBi exhibit nontrivial topological characteristics [16]. However, imaginary frequency modes were observed in the phonon spectrum of their pristine structures. It has been found that low buckled structure and passivation including halogenation, hydrogenation and methyl-functionalization stabilize the structure and increase the bandgap [17-26]. Especially, the hydrogen bonds can also simulate the electronic structure with the effect of a substrate and efficiently identify the quantum spin Hall phase of these 2D materials. Moreover, functionalized III-Bi monolayers can realize nontrivial topological states preferably compared with the pristine structures.

However, several theoretical calculations were made for the ground-state properties of InBi, AlBi and GaBi [27], the present study extends these investigations of the electronic structure of InBi, AlBi and GaBi using positrons.

In this paper, we investigate theoretically the positron annihilation and its effect in InBi, AlBi and GaBi compounds. The technique of angular correlation of positron annihilation radiation (ACAR) has become a well-established method for measuring the electron momentum distributions in solids, since the annihilation radiation carries information on the electron momenta [28]. Several measurements on the electron momentum distribution in Ge [29,30] have been made in the past few decades. The investigation of the electronic structure of solids using positrons occupies a place of increasing importance in solid state physics. The recent growth in positron studies of defect trapping in semiconductors suggests the desirability of an improved theoretical understanding of the annihilation parameters for such systems.

This paper is organized as follows: In Section 2, we describe the computational approach used in this work. The results for InBi, AlBi and GaBi are presented and discussed in Section 3. Finally, we present a brief conclusion.

II-FORMALISM

In the independent particle approximation, the probability of annihilation of the electron-positron pair with momentum **p** is given by:

$$\Gamma(\mathbf{p}) = const\sum_{n}\sum_{k}^{occ.}\left|\int_{\Omega}\psi_{n\mathbf{k}}(\mathbf{r})\phi(\mathbf{r})\exp(-i\mathbf{pr})d\mathbf{r}\right|^2 \quad (1)$$

where $\psi_{n\mathbf{k}}$ is the Bloch wave function of the valence electron with wave vector $\boldsymbol{k}$ in the n-th band, and ϕ is the Bloch wave function of the thermalized positron. The integration is performed over the whole volume of the crystal and the summation is taken over the occupied electronic states. By assuming that the positron is fully thermalized, we regard **p** as the momentum of the valence electron.

The counting rate measured by the standard parallel slit apparatus is proportional to

$$\Gamma(p_x, p_y) = \int dp_z \Gamma(p_x, p_y, p_z) \quad (2)$$

We define the function $N(\mathbf{p})$ by folding $\Gamma(\mathbf{p})$ with respect to all reciprocal lattice vectors $\mathbf{G}$ as follows:

$$N(\mathbf{p}) = \sum_{\mathbf{G}}(\mathbf{p}+\mathbf{G}) \quad (3)$$

We have exactly

$$N(\mathbf{p}) = const\sum\int d\mathbf{k}\delta(\mathbf{k}-\mathbf{p}+\mathbf{G})\frac{1}{\Omega}\int_{\Omega}\left|U_{n\mathbf{k}}(\mathbf{r})\right|^2\left|V(\mathbf{r})\right|^2 d\mathbf{r} \quad (4)$$

Where $U_{n\mathbf{k}}$ and V are the periodic parts of the wave function of valence electron and positron, respectively, and the **r**-integration is performed over the unit cell with volume Ω.

In the folded function $N(\mathbf{p})$, each $\mathbf{k}$-point in the momentum space occupied by the electrons is mapped by the δ-function in the weight of the electron-positron overlap in their densities. Corresponding to the experimental condition, $N(\mathbf{p})$ is one dimensionally integrated along the direction towards a fixed detector of γ-rays as

$$N(p_x, p_y) = \int dp_z N(p_x, p_y, p_z), \quad (5)$$

the mapping of the $N(p_x, p_z)$ on the $p_x - p_y$ plane gives information about the occupied $\mathbf{k}$-space.

If the positron wave function is assumed to be constant (namely a uniform distribution of positrons), we obtain the exact geometry of the occupied $\mathbf{k}$-space along the direction of integration, namely the projection of the first Brillouin zone, for semiconductors the real non-uniform distribution of positrons deforms the geometry, according to the weight of the electron-positron overlap .

For the calculation of the weight function, we adopted the pseudo-potential method, where the periodic parts $U_{n\mathbf{k}}$ and $V(\mathbf{r})$ are expanded in terms of the plane waves,

$$U(\mathbf{r}) = \sum_{\mathbf{R}} C_{n\mathbf{k}} \exp(i\mathbf{Rr}) \quad \text{for valence electrons,} \quad (6)$$

$$V(\mathbf{r}) = \sum_{G} D(\mathbf{G})\exp(i\mathbf{Gr}) \quad \text{for positrons,} \quad (7)$$

Where **R**'s and **G**'s are the reciprocal lattice vectors. The weight function is expressed as follows:

$$\frac{1}{\Omega}\int\left|U_{n\mathbf{k}}(\mathbf{r})\right|^2\left|V(\mathbf{r})\right|^2 d\mathbf{r} = \sum_{\mathbf{R}'}\sum_{\mathbf{R}}\sum_{\mathbf{G}'}\sum_{\mathbf{G}} C_{n\mathbf{k}}(\mathbf{R}')C_{\mathrm{nk}}(\mathbf{R})D(\mathbf{G}')D(\mathbf{G})\delta_{\mathrm{k+k'+G-G'}} \tag{8}$$

the $C_{n\mathbf{k}}(\mathbf{R})'s$ and $D(\mathbf{G})'s$ were determined in the following energy band calculations.

The object of each band structure calculation, be it for an electron or a positron, is to solve the Schrödinger equation for a crystal potential *V(r),*

For the valence electrons we have

$$H\psi_{n\mathbf{k}}(\mathbf{r}) = E\psi_{n\mathbf{k}}(\mathbf{r}), \tag{9}$$

$$H = \frac{p^2}{2m} + V_{pseudo}, \tag{10}$$

where the V_{pseudo} is the empirical pseudo-potential determined by Kobayashi [32]. The form factors used in our calculations were taken from [33].

For the positron we have

$$H\phi(\mathbf{r}) = E\phi(\mathbf{r}), \tag{11}$$

$$H = \frac{p^2}{2m} + V_{\text{ionic core}} + \boldsymbol{V}_{\text{valence electrons}}, \tag{12}$$

where the $V_{\text{ionic core}}$ is the crystal ionic potential given by

$$V_{\text{ionic core}}(\mathbf{r}) = \sum_i\sum_j v(\mathbf{r} - \mathbf{R_i} - \mathbf{t_j}); \tag{13}$$

Here, in the point core approximation we adopted

$$V(\mathbf{r}) = \frac{Ze^2}{r}, \tag{14}$$

and the potential due to the valence electrons is

$$V_{\text{valence electrons}} = -e^2\int\frac{\rho(\mathbf{r}')d\mathbf{r}}{|\mathbf{r}-\mathbf{r}'|}. \tag{15}$$

The density of the valence electrons $\rho(\mathbf{r})$ is evaluated by using $\psi_{n\mathbf{k}}(\mathbf{r})$ as

$$\rho(\mathbf{r}) = 2\sum_n\sum_{\mathbf{k}}\left|\psi_{\mathbf{nk}}(\mathbf{r})\right|^2. \tag{16}$$

The wave function of the fully thermalized positron ϕ is given, in good approximation, by the wave function $\phi_{\boldsymbol{n}=1,\boldsymbol{k}=0}$, i.e. the wave function at the bottom of the positron energy band.

The two-photon momentum density $\rho^{2\gamma}(\mathbf{p})$ for positron annihilation is given, in the IPM, by:

$$\rho^{2\gamma}(\mathbf{p}) = \sum_{n,k} \eta_n(\mathbf{k}) \left| \int d^3\mathbf{r} \exp(-i\mathbf{pr}) \psi_{nk} \phi(\mathbf{r}) \right|^2 \tag{17}$$

where $\eta_n(k)$ is the occupation number equal to 1 for the occupied states and zero for the empty states. For periodic potential at zero temperature Eq. (17) will be reduced to:

$$\rho^{2\gamma}(\mathbf{p}) = \sum_{n,k} \sum_{G} \eta_n(\mathbf{k}) \left| A_{n,k}(\mathbf{G}) \right|^2 \delta(\mathbf{p} - \mathbf{k} - \mathbf{G}) \tag{18}$$

where $A_{n,k}(\mathbf{G})$ are the Fourier coefficients of the positron-electron wave function product.

It is usual to perform a "Lock-Crisp-West" (LCW) zone folding [27] of the various extended zone components of $\rho(\mathbf{p})$ into the first Brillouin zone, thus forming the zone-reduced momentum density:

$$n(k) = \sum_{G_i} \rho(\mathbf{p} + \mathbf{G_i}) \tag{19}$$

where $\mathbf{G_i}$ is the *i*-th reciprocal lattice vector defined within the first Brillouin zone. Using Block's theorem, $n(k)$ can be described as:

$$n(k) = const \sum_{n} \theta(E_F - E_{n,k}) \int \left| \psi_{n,k}(\mathbf{r}) \phi(\mathbf{r}) d\mathbf{r} \right|^2 \tag{20}$$

where E_F is the Fermi energy and $\theta(E_F - E_{n,k})$ is a step function as follows:

$$\theta(E_F - E_{n,k}) = \begin{cases} 1 & E_F \le E_{n,k} \\ 0 & E_F \ge E_{n,k} \end{cases} \tag{21}$$

For the metallic material, the two photon momentum distribution exhibits break at the Fermi momentum **p=k** and also another at **p=k+G**.

However, in the long slit angular correlation experiment one measures a component of the pair momentum density as given by:

$$N(p_z) = \iint \rho^{2\gamma}(\mathbf{p}) dp_x dp_y \tag{22}$$

It contains two sets of information. The sharp breaks in $N(p_x, p_y)$ reveal the topology and size of the Fermi surface (FS) while the shape of $N(p_x, p_y)$ reflects more details of the wave functions of the electron and the positron.

3 Results & Discussions

The positron band structures, as calculated by the IPM approximation, are shown in **figures 1**(a), 1(b) and 1(c), the first obvious observation is the similarity between the positron and electron energy spectrum, with the exception that the positron energy spectrum does not exhibit a band gap. The lowest positron energy state is the Γ_1 state at k_+=0. The Γ_1 state of InBi lies above that of AlBi and GaBi. The electron and positron band structures are almost free electron like; the electron and the positron see the same symmetry operations; we therefore expect merely the same energy band forms.

We computed the positron charge densities at the bottom of the lowest band. These charge densities are calculated along the normal nearest-neighbor tetrahedral distance (the <111> axis) and in the ($11\bar{1}$) plane. Positron charge densities at Γ_1 for InBi, AlBi and GaBi are displayed in **figures** (2, 3(a), (3(b) and 3(c)). Qualitatively, these charges present nearly the same characteristics, the important feature in all compounds is the remarkable shift of the positron charge density towards the Se,

Te and S atom, there is however a clear buildup of positron charge distribution in the interstitial regions, and that the probability is low around the positions of the nuclei.

From a quantitative point of view, there is a difference of charge in the interstitial regions, the positron distribution is more pronounced in the neighborhood of the Te anion than in that of the Se and S cations, the driving force behind the displacement of the bonding charge is considered as the ability of the Te, Se and S to attract electrons compared to Zn atoms on the lowest row of the periodic table.

Note the asymmetrical positron distribution for InBi, AlBi and GaBi, while the positron charge is symmetrically distributed in elemental semiconductors [31], note also the difference in the positron density at the atomic cores for InBi, AlBi and GaBi, that of InBi is slightly larger than that of AlBi and GaBi. These differences in profiles are immediately attributable to the cell which contains the larger valence and the larger ion core, due to the fact that In presents a larger valence than Ga and Al. The conclusion would be that the positron charge distribution is sensitive to the change in the valence charge density and the contribution of the core electrons results in a higher repulsion of positrons. We are considering the implications of this in regard to the propensity for positron trapping. The positronic contour plots for InBi, AlBi and GaBi look rather similar.

Figures 4 and 5 display sections of the 2D electron-positron momentum densities by integration of the appropriate plane [001] and [110] directions for InBi, AlBi and GaBi. The general feature of the observed 2D momentum distribution of annihilation radiation is similar. The electron-positron momentum density in the [001] directions is seen to be flat as observed in Si and Ge [32]. Compared to this, the profile along the <110> direction is sharply peaked. The sharp peaking along the <110> direction and the flatness of the peak along the <001> direction could be understood in terms of the contribution of σ and π* orbitals to the ideal sp3 hybrid ones. From the quantitative point of view, we note however, that the e-e^+ momentum density is more pronounced in InBi than in AlBi and GaBi, this is consistent with the electronic configurations of outer electrons as mentioned above. This is manifested in the angular correlation curve as an increase in the fractional area of the broad component of the momentum.

4 Conclusion

We have shown that by performing the e^-e^+ charge density and momentum densities calculations, a deep insight into the electronic properties can be achieved. The positron charge distribution is sensitive to the change in the valence charge density and the contribution of the core electrons which results in a higher repulsion. Our results will lead us to think that the positron may preferentially annihilate with the anion rather than the cation and we may also deduce that positrons are attracted by sites with high electronic charge densities.

References

[1] A. Bansil, H. Lin and T. Das, Rev. Mod. Phys., 2016, 88, 21004.

[2] N. Nagaosa, J. Sinova, S. Onoda, A. H. MacDonald and N. P. Ong, Rev. Mod. Phys., 2010, 82, 1539.

[3] H. Weng, R. Yu, X. Hu, X. Dai and Z. Fang, Adv. Phys., 2015, 64, 227–282

[4] B. Yan and S.-C. Zhang, Rep. Prog. Phys., 2012, 75, 96501

[5] J. E. Moore, Nature, 2010, 464, 194–198

[6] M. Z. Hasan and C. L. Kane, Rev. Mod. Phys., 2010, 82, 3045

[7] X.-L. Qi and S.-C. Zhang, Rev. Mod. Phys., 2011, 83, 1057

[8] B. A. Bernevig and S.-C. Zhang, Phys. Rev. Lett., 2006, 96, 106802

[9] C. L. Kane and E. J. Mele, Phys. Rev. Lett., 2005, 95, 226801

[10] C.-C. Liu, W. Feng and Y. Yao, Phys. Rev. Lett., 2011, 107, 76802

[11] C.-C. Liu, H. Jiang and Y. Yao, Phys. Rev. B: Condens. Matter Mater. Phys., 2011, 84, 195430

[12] W. Qiu, H. Ye, Z. Yu and Y. Liu, Superlattices Microstruct., 2016, 97, 250–257

[13] L. Fu, C. L. Kane and E. J. Mele, Phys. Rev. Lett., 2007, 98, 106803

[14] L. Fu and C. L. Kane, Phys. Rev. Lett., 2009, 102, 216403

[15] X.-L. Qi, T. L. Hughes and S.-C. Zhang, Phys. Rev. B: Condens. Matter Mater. Phys., 2008, 78, 195424

[16] F.-C. Chuang, L.-Z. Yao, Z.-Q. Huang, Y.-T. Liu, C.-H. Hsu, T. Das, H. Lin and A. Bansil, Nano Lett., 2014, 14, 2505–2508

[17] C. P. Crisostomo, L.-Z. Yao, Z.-Q. Huang, C.-H. Hsu, F.-C. Chuang, H. Lin, M. A. Albao and A. Bansil, Nano Lett., 2015, 15, 6568–6574

[18] Y. Ma, Y. Dai, L. Kou, T. Frauenheim and T. Heine, Nano Lett., 2015, 15, 1083–1089

[19] S. Li, W. Ji, C. Zhang, S. Hu, P. Li, P. Wang, B. Zhang and C. Cao, Sci. Rep., 2016, 6, 23242

[20] Y. Kim, W. S. Yun and J. D. Lee, Sci. Rep., 2016, 6, 33395

[21] R. R. Q. Freitas, F. de Brito Mota, R. Rivelino, C. M. C. de Castilho, A. Kakanakova-Georgieva and G. K. Gueorguiev, Nanotechnology, 2016, 27, 55704

[22] Y. Ma, X. Li, L. Kou, B. Yan, C. Niu, Y. Dai and T. Heine, Phys. Rev. B: Condens. Matter Mater. Phys., 2015, 91, 235306

[23] L. Li, X. Zhang, X. Chen and M. Zhao, Nano Lett., 2015, 15, 1296–1301

[24] S.-P. Chen, Z.-Q. Huang, C. P. Crisostomo, C.-H. Hsu, F.-C. Chuang, H. Lin and A. Bansil, Sci. Rep., 2016, 6, 31317

[25] R. R. Q. Freitas, F. de Brito Mota, R. Rivelino, C. m. c. De Castilho, A. Kakanakova-Georgieva and G. K. Gueorguiev, Phys. Rev. B: Condens. Matter Mater. Phys., 2015, 27, 485306

[26] R. R. Q. Freitas, R. Rivelino, F. de Brito Mota, C. M. C. de Castilho, A. Kakanakova-Georgieva and G. K. Gueorguiev, J. Phys. Chem. C, 2015, 119, 23599–23606

[27] Nor Ashwani Abdul Rahim et al, Computational Materials Science Volume 114, (2016), 40-46

[28] A. Talmantaite, M. r. c. Hun & B. G. Mendis Journal of Microscopy, Vol. 00, Issue 0 2020, pp. 1–4

[29] J. Makkonen and Filip Tuomisto, J. Appl. Phys. 135, 040901 (2024)

[30] Wagner Tenfen, Josiney de Souza Glória, Sarah Esther da Silva Saab, Eliton Popovicz Seidel and Felipe Arretche, Hydrogen 2025, 6(1)

[31] J M Campillo Robles, E Ogando2 and F Plazaola, Journal of Physics: Condensed Matter 19, 17 (2007) 176222-176242

[32] Shuji Hasegawa 2024 Appl. Phys. Express 17 050101

Captions of Figures and Tables

Figure 1(a): Positron energy band structure along principal symmetry lines for InBi.

Figure 1(b): Positron energy band structure along principal symmetry lines for AlBi.

Figure 1(c): Positron energy band structure along principal symmetry lines for GaBi.

Figure (2): The thermalized positron charge density in InBi, AlBi and GaBi at the

Γ_1 point along >111< direction.

Figure 3(a): The thermalized positron charge density in InBi at Γ_1 point in the (110) plane.

Figure 3(b): The thermalized positron charge density in AlBi at Γ_1 point in the (110) plane.

Figure 3(c): The thermalized positron charge density in GaBi at Γ_1 point in the (110) plane.

Figure 4: The integrated electron-positron momentum density in InBi, AlBi and GaBi along the >001< direction.

Figure 5: The integrated electron-positron momentum density in InBi, AlBi and GaBi along the >110< direction.

Figure 6(a): The calculated electron -positron momentum densities for InBi in the (001-110) plane.

Figure 6(b): The calculated electron -positron momentum densities for AlBi in the (001-110) plane.

Figure 6(c): The calculated electron -positron momentum densities for GaBi in the (001-110) plane.

Figure 7(a): The calculated electron-positron momentum density after LCW folding in InBi.

Figure 7(b): The calculated electron-positron momentum density after LCW folding in AlBi.

Figure 7(c): The calculated electron-positron momentum density after LCW folding in GaBi.

Figure 8(a): The calculated electron -positron momentum densities for InBi in the (001-110) plane (bird's eye view).

Figure 8(b): The calculated electron -positron momentum densities for AlBi in the (001-110) plane (bird's eye view).

Figure 8(c): The calculated electron -positron momentum densities for InBi in the (001-110) plane (bird's eye view).

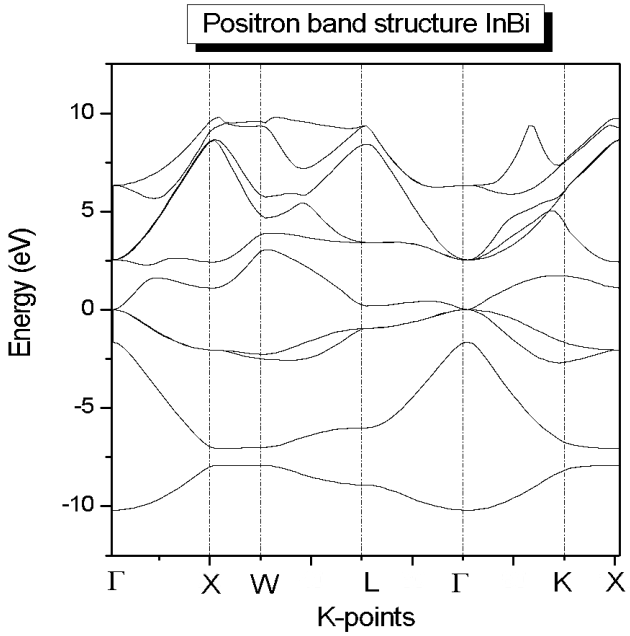

Figure 1a

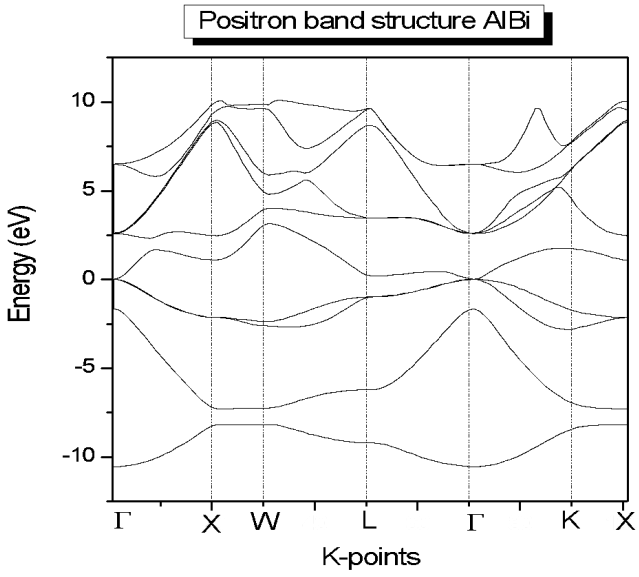

Figure 1b

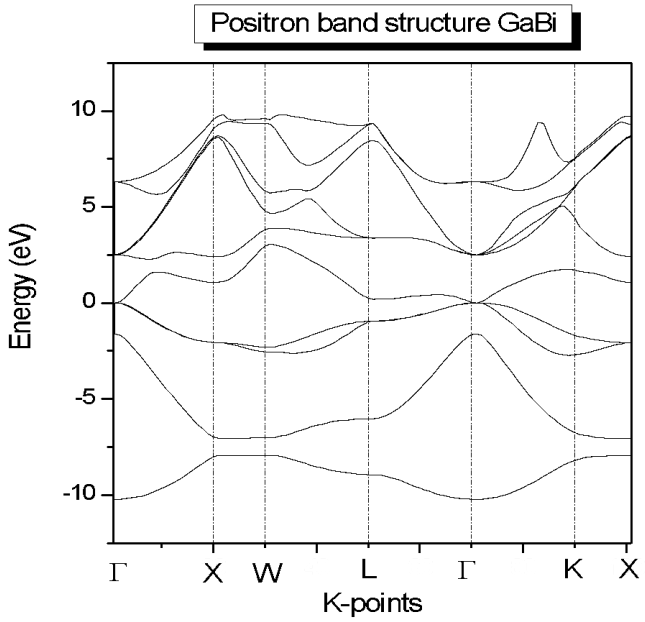

Figure 1c

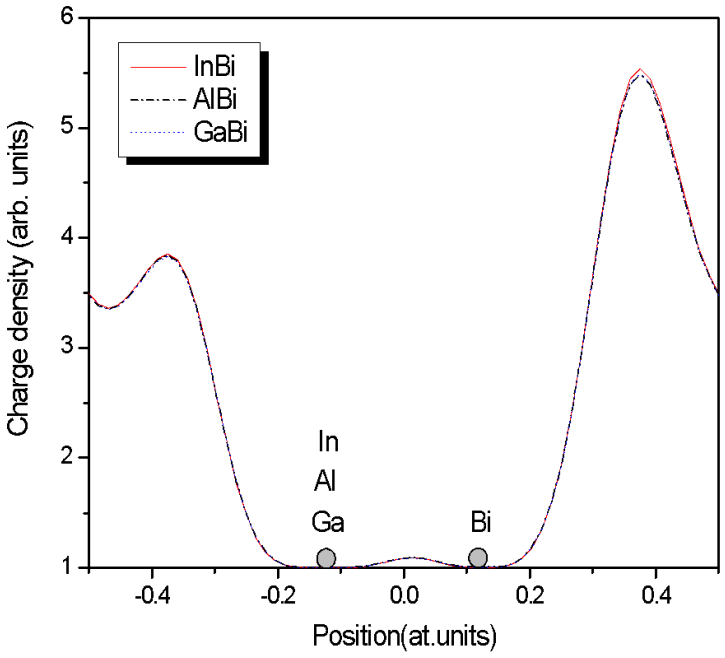

Figure 2

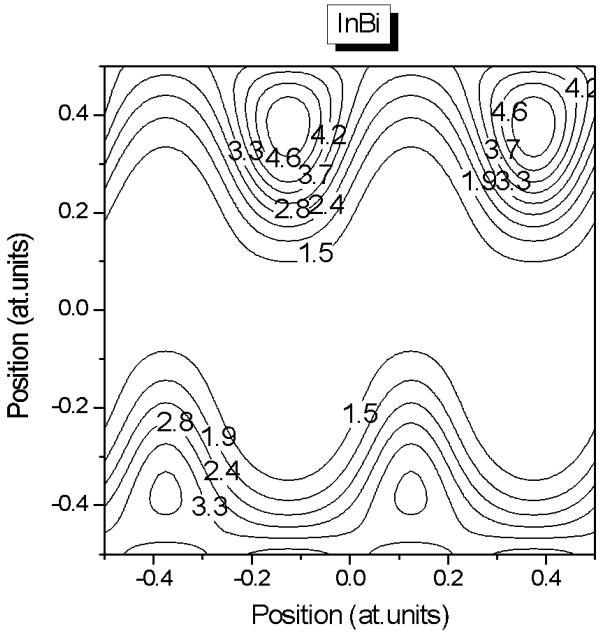

Figure 3a

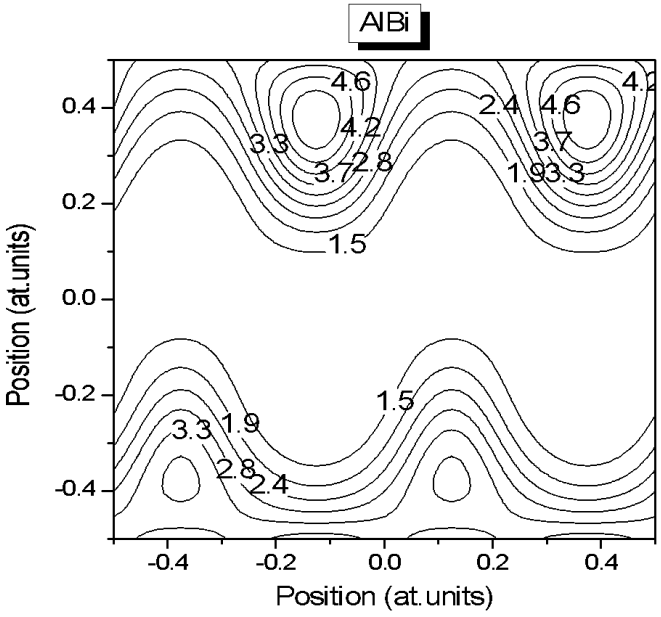

Figure 3b

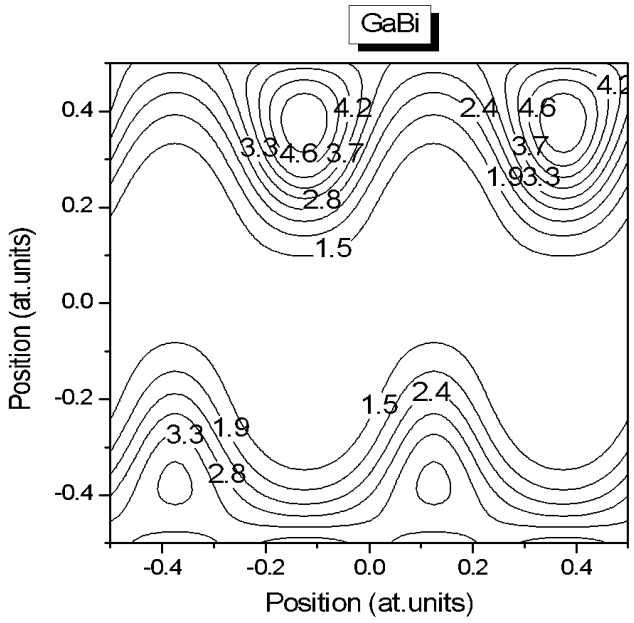

Figure 3c

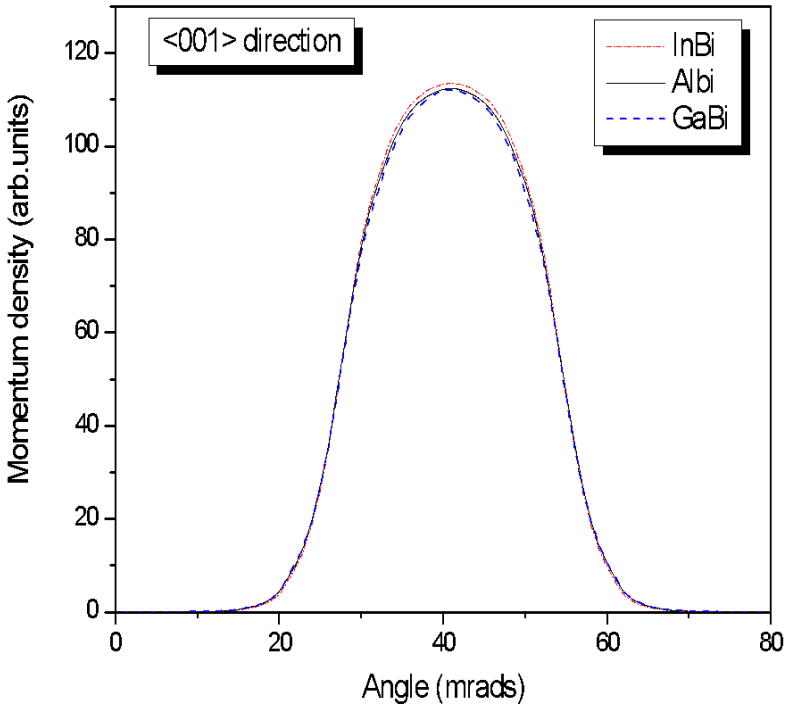

Figure 4

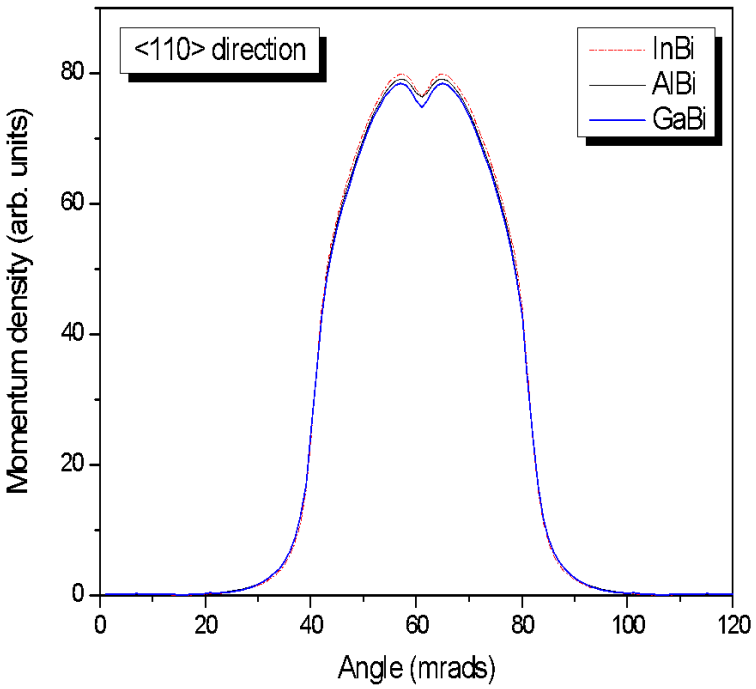

Figure 5

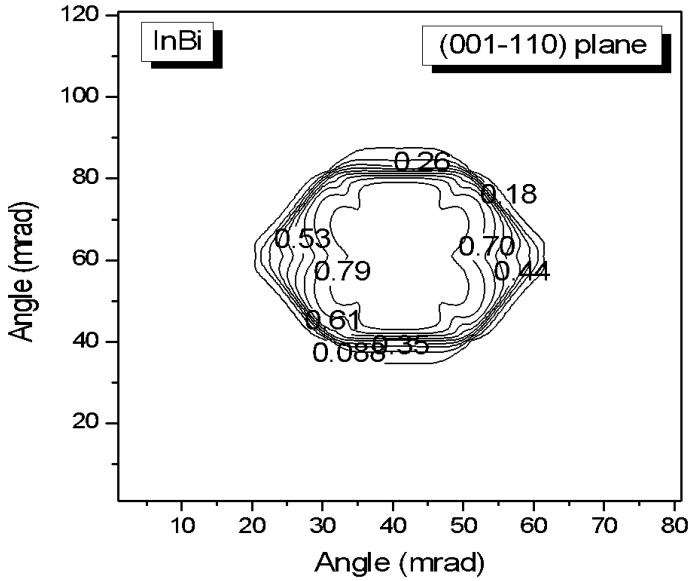

Figure 6a

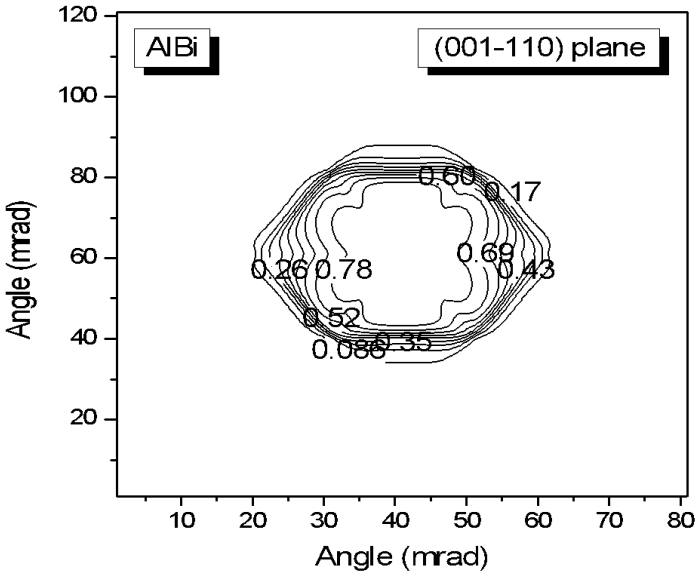

Figure 6b

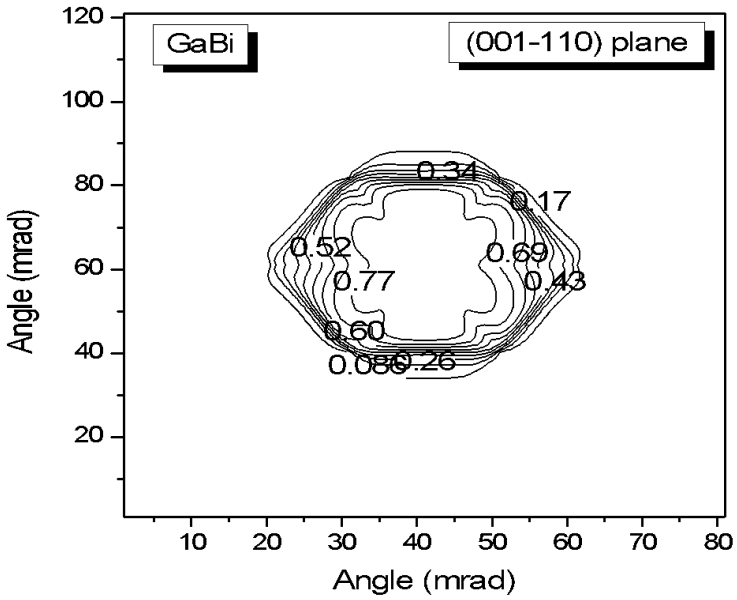

Figure 6c

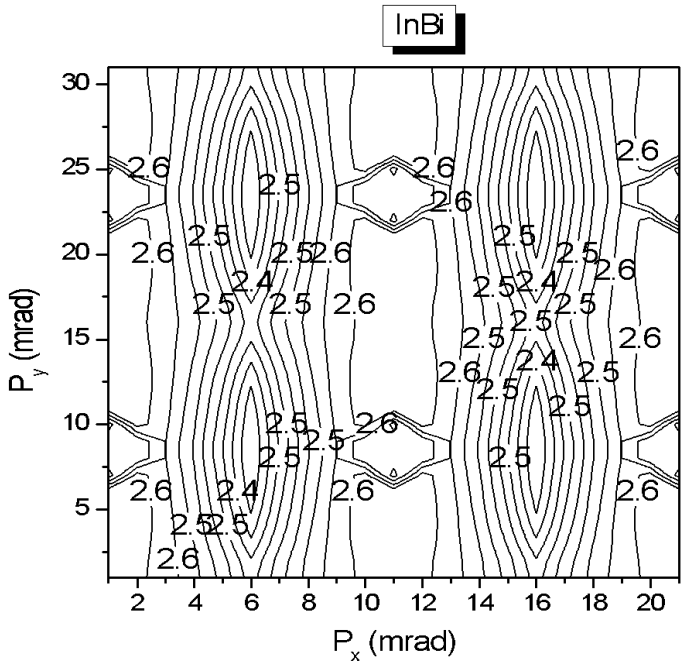

Figure 7a

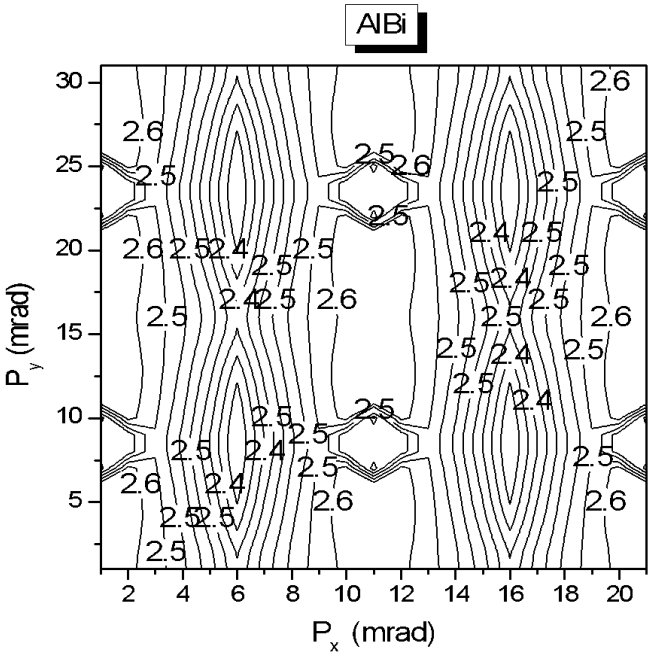

Figure 7b

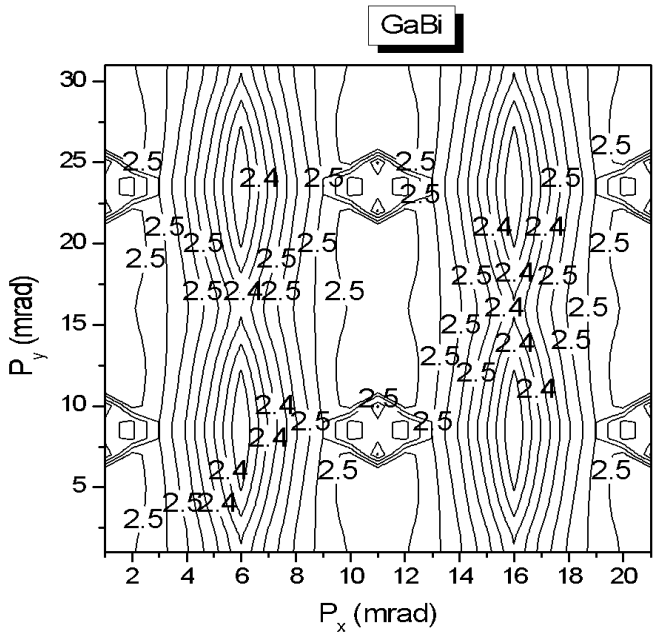

Figure 7c

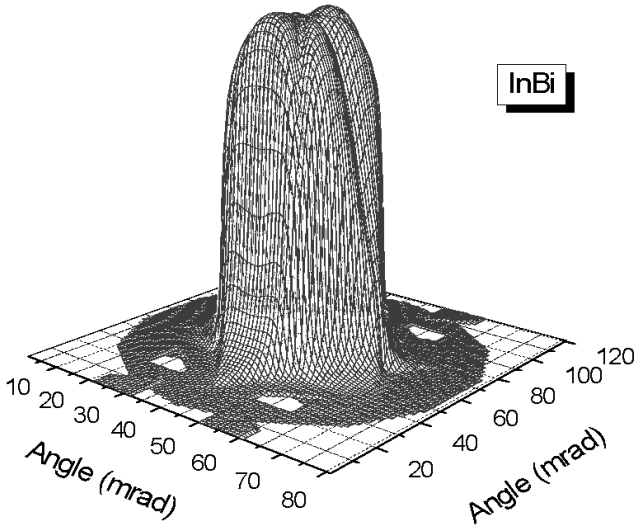

Figure 8a

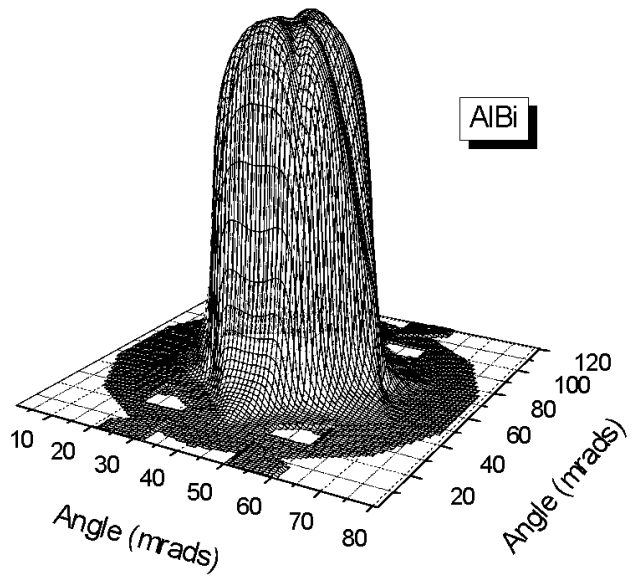

Figure 8b

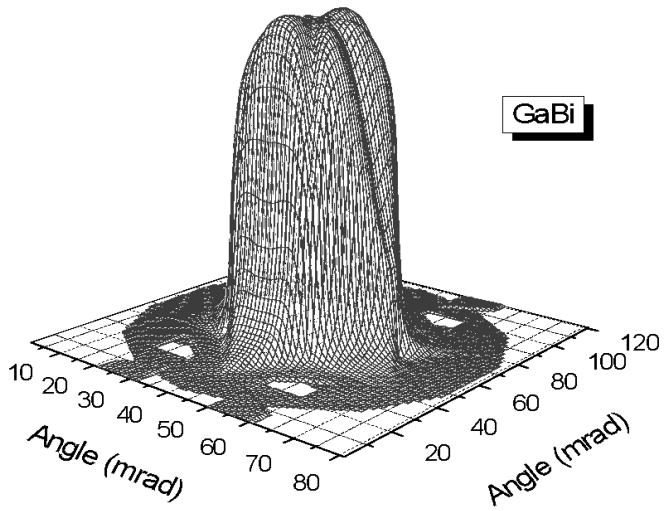

Figure 8c

Tables

Table 1: The adjusted symmetric and antisymmetric form factors (in Ry), and the lattice constant a_o (in atomic units) for ZnSe, ZnTe and ZnS used in these calculations.

compound	Adjusted lattice constant a_o	Calculated lattice constant a_o [4]	Adjusted form factors
ZnSe	10.67851	10.66321	$V_s(3)$=-0.218 $V_s(8)$=0.029 $V_s(11)$=0.064 $V_a(3)$=0.139 $V_a(4)$=0.062 $V_a(11)$=0.016
ZnTe	11.4723	11.4622	$V_s(3)$=-0.22 $V_s(8)$=0.0 $V_s(11)$=0.05 $V_a(3)$=0.13 $V_a(4)$=-0.1 $V_a(11)$=-0.01
ZnS	10.2249	10.2130	$V_s(3)$=-0.25789 $V_s(8)$=0.03 $V_s(11)$=0.07416 $V_a(3)$=0.20743 $V_a(4)$=0.14 $V_a(11)$=0.04